Quantum Size Effect on Surface Photovoltage Spectra: Alpha-Fe_2O_3 Nanocrystals on the Surface of Monodispersed Silica Microsphere

K. Cheng

Institute of Physics, Chinese Academy of Sciences, Beijing 100080, China, and Lab for Special Functional Materials, Henan University, Kaifeng 475001, P. R. China

Y. P. He, Y. M. Miao, B. S. Zou,* Y. G. Wang, and T. H. Wang

Micro-Nano Technologies Research Center, Hunan University, Changsha 410082, P. R. China, and Institute of Physics, Chinese Academy of Sciences, Beijing 100080, P. R. China

X. T. Zhang and Z. L. Du*

Lab for Special Functional Material, Henan University, Kaifeng 475001, P. R. China

Received: December 31, 2005; In Final Form: February 19, 2006

A new method for the preparation of Fe_2O_3 nanoparticle/SiO_2 microsphere composites is described, in which fine alpha-Fe_2O_3 nanocrystals were prepared by forced hydrolysis of $FeCl_3$ aqueous solution. The structure and optical spectra of these alpha-Fe_2O_3 nanocrystals have been studied. Their visible optical absorption can be enhanced by their adsorptions on the surface of SiO_2 microspheres and thereafter simple packing of these microspheres to the aggregated structures. The size-dependent photogenerated surface photovoltage spectra (SPS) of these composites were studied, and quantum confinement effects of the SPS properties were observed. The transport of photoinduced charges between nanocrystals with intrinsic electronic nature of confined states accounts for this phenomenon. These results are helpful in understanding the relationship among d−d transition and charge-transfer transition in transition metal oxides and find applications in photovoltaic devices.

Introduction

Recently there has been substantial interest in the preparation and characterization of semiconductor nanoparticles, owing to their potential applications in solar energy conversion, photocatalysis, and in optoelectronic fields. These semiconductor nanoparticles can exhibit size-dependent electronic, optical, magnetic, and chemical properties.[1−3] Among them, nanometer-sized transition metal oxide (TMOs) nanoparticles have also attracted much attention for their potential technological applications ranging from ultrahigh-density magnetic storage and colossal magnetic resistance to biological imaging contrast agents and nanocatalysts, because their unique and special physicochemical properties can be tuned according to size (quantum size effect), composition, and surface modification.[4,5] The interaction and transformation between spin, charge, and orbital in confined space are crucial to the properties of these materials and structures.

Alpha-Fe_2O_3 is an antiferromagnetic oxide with canting ferromagnetic responses at room temperature. However, its high stability and semiconducting properties enable its use as a photocatalyst. There are reports on its photovoltaic properties.[6] Although it cannot work as a good solar conversion material, the size-dependent semiconducting and photoelectric properties of alpha-Fe_2O_3 need to be understood.[7]

Presently, there are some complicated or controversial theoretical and experimental descriptions of the electronic structure of TMO nanomaterials. A critical obstacle facing TMO nanomaterials is their instinctive tendency to conglomerate and grow during preparation and subsequent processing steps.[8,9] Of course, TMOs can be stabilized by surface modification using polymers, organic ligands, or surfactants; however, such stabilization techniques affect the electronic transport properties. Avoiding TMO agglomeration is important for the study of the electronic properties, and one strategy to do this is to incorporate the nanoparticles into a polymer, a glass, or ceramic.[10] Pedro Tartaj et al. found that, for sufficiently dilute dispersions, interparticle interactions (usually of a dipolar nature) are negligible,[11] and they dispersed Fe_2O_3 nanoparticles in submicrometer spherical silica particles using a complicated aerosol-assisted method to study their magnetic properties. Of course, many other semiconductor nanocrystals and their optical properties have been studied in dispersed matrices, as reported in the literature.[1−5]

We report here a novel and easy method to fabricate alpha-Fe_2O_3 on the surface of monodispersed silica spheres. The alpha-Fe_2O_3 nanoparticles in such a system are contacting each other. We studied the relationship between size and photogenerated charge separation properties through the surface photovoltage spectrum (SPS) and illustrate how particle size effect can influence the physical properties of alpha-Fe_2O_3. This should be useful for the practical application of alpha-Fe_2O_3 nanoparticles in solar cells and for photocatalysis.

Traditional Theory of SPS

Generally, the photovoltaic effect in bulk semiconductors comprises an illumination-induced change in the equilibrium potential distribution and is typically the result of some charge transfer and redistribution within the device due to the incident illumination.[12] There are several situations. One of the photovoltaic phenomena comes from the potential difference induced

10.1021/jp057593q CCC: $33.50
Published on Web 03/24/2006

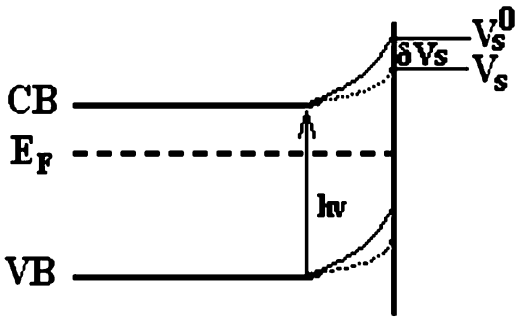

Figure 1. Schematic representations of energy band variation of an n-type semiconductor with a Schottky-type barrier before and after photoexcitation.

by internal carrier redistribution after pulse laser photoexcitation in a scalable time. Another specific photovoltaic effect is the surface photovoltaic effect as shown in Figure 1.[13,14]

The SPS method is a well-established contactless and nondestructive technique for semiconductor characterization. This method has a very high sensitivity of about 10^8 q/cm^2, or about one elementary charge per 10^7 surface atoms.[15] This technique has been successfully used to study the charge transfer effect in photoinduced surfaces, dye-sensitization processes, and photocatalysis, etc.[16,17]

For photoinduced photovoltaic effects in a system containing quantum-confined nanocrystal aggregates, the above two situations cannot occur, because the particle size is much smaller than the band bending distance and the electronic mean free path in bulk, or is comparable to them. At this moment, there occurred the fast trapping of electron and hole on the surface and local excitation after photoexcitation,[18−20] so the related electron−hole separations are dependent on the nanoparticle couplings or on the aggregate structures of nanocrystals.

Experimental Section

Materials. Ferric chloride hexahydrate ($FeCl_3 \cdot 6H_2O$ > 99%), hydrochloric acid (HCl), tetraethoxysilane (TEOS), ammonium hydroxide, and ethanol were purchased from Beijing chemical reagent company used without further purification. Doubly distilled water was used for the process.

Sample Preparation. Fine alpha-Fe_2O_3 nanoparticles were prepared by a traditional method: forced hydrolysis of $FeCl_3$ aqueous solution in open vessel.[21,22] Specifically, predetermined amounts of stock solution of $FeCl_3 \cdot 6H_2O$ (3 mol dm^{-3}) and HCl (0.2 mol dm^{-3}) were mixed in a three-necked bottle at the ratio of 1:3 (V/V), and deionized water was added until the final concentration of Fe^{3+} was 0.01 mol dm^{-3}. This mixture was refluxed at about 100 °C for 2 h, and then cooled to room temperature. The obtained reddish-brown transparent sol was dialyzed using a dialysis bag in deionized water to remove Cl^- ions. The deionized water was changed twice a day. Two days later, we obtained a stable alpha-Fe_2O_3 hydrosol with deep red color. The Fe_2O_3 particle size can be tuned by adjusted the amount of $FeCl_3$ and aging conditions.[23] Silica nanospheres were fabricated according to the well-known Stŏber method by hydrolysis and condensation of tetraethoxysilane (TEOS) in a mixture of ethanol with water, using ammonia as catalyst to initiate the reaction.[24] In a typical experiment, 7 mL TEOS was dissolved in 100 mL absolute ethanol. Then 6 mL H_2O and 7 mL NH_4OH (26−28wt% in H_2O) were rapidly injected under vigorous stirring at room temperature. The stirring process was continued for 4 h. The colloidal silica spherical particles have an average size 170 nm in diameter. Because the newly prepared silica colloidal particles are negative,[25] when mixed with the alpha-Fe_2O_3 solution the alpha-Fe_2O_3 will adhere on the surface of silica spherical particles due to the positive charge of alpha-Fe_2O_3 nanoparticles under acidic conditions.[26] The composite precipitate was then obtained by centrifuging. The precipitate was washed and dried in the oven at 60 °C. In this way we get three kinds of composite of silica microspheres with alpha-Fe_2O_3 nanoparticles of 5, 12, and 48 nm, marked as samples A, B, and C, respectively.

Characterization. The morphologies of SiO_2 and Fe_2O_3/SiO_2 were obtained with a JEM 100 CX-II transmission electron microscope. The structural properties were analyzed by X-ray powder diffraction (XRD) with a Bruker M18XHF diffractometer using the monochromatized X-ray beam from the Cu K_α radiation. The optical reflectance and absorption spectra in the range of 250∼900 nm of the samples were measured using a TU-1901 UV−visible spectrophotometer with an integrating sphere. The spectra were referenced against the compressed $BaSO_4$ powders. The SPS measurements were carried on homemade SPS equipment. Monochromatic light was obtained by passing light from a 500 W xenon lamp through a monochromator. A lock-in amplifier (SR830-DSP, made in the USA) synchronized with a light chopper was employed to amplify the photovoltage signal. The spectral resolution is 1 nm. The SPS and absorption spectral intensities are all normalized with that of the light resources.

Results and Discussion

A. Morphology and Structure of the Composite. The representative TEM images of 5 nm alpha-Fe_2O_3 coated on the surface of SiO_2 spheres is given in Figure 2. From Figure 2A, we can see that the average particle size of alpha-Fe_2O_3 was about 5 nm. Figure 2B is the uncoated SiO_2 spheres. They are nearly monodispersed spheres with a diameter $d_{sphere} = 170 \pm 10$ nm. Figure 2C and Figure 2D show the TEM images of alpha-Fe_2O_3 nanocrystals adsorbed on the surface of SiO_2 microspheres taken at a low magnification and high magnification, respectively. We can see clearly the alpha-Fe_2O_3 nanocrystals adsorbed on the surface of SiO_2 spheres. Figure 3 shows the X-ray diffraction patterns of the prepared 48 nm alpha-Fe_2O_3 along with the standard one. From this pattern, it is clear that synthesized alpha-Fe_2O_3 nanoparticles have a single phase with the crystal structures reported by the Joint Committee on Powder Diffraction Standards (JCPDS file No 33-0664).

B. UV−Vis Diffuse Reflectance Spectroscopy. Figures 4a and 4b illustrate the absorption spectra of 1.2 wt % alpha-Fe_2O_3/SiO_2 samples and free-standing Fe_2O_3 nanocrystals by reflectance techniques. According to references 27 and 28, the absorption between 250 and 400 nm results from the ligand-to-metal charge-transfer transitions and less contribution comes from the Fe^{3+} ligand field transitions $^6A_1 \rightarrow {}^4T_1(^4P)$ at 290∼310 nm, $^6A_1 \rightarrow {}^4E(^4D)$, and $^6A_1 \rightarrow {}^4T_2(^4D)$ at 360 ∼ 380 nm. Region 2 (400∼600 nm) is assigned to the pair excitation processes $^6A_1 + {}^6A_1 \rightarrow {}^4T_1(^4G) + {}^4T_1(^4G)$ at 485∼550 nm, possibly overlapping the contributions of the $^6A_1 \rightarrow {}^4E, {}^4A_1(^4G)$ ligand field transitions at 430 nm and the charge-transfer band tail (extended from the band of 200−400 nm to visible). Generally, the UV absorption intensity of Fe_2O_3 nanocrystal sol is greater than that in the visible region, because the former one is allowed transition while the d−d transition is forbidden as in Figure 4b. As is well known, light scattering for visible light takes effect in the absorption spectra if the particle size becomes greater than 20 nm.[29] This means that larger particles should show stronger reflectivity and the reflectivity of particles should shift to longer

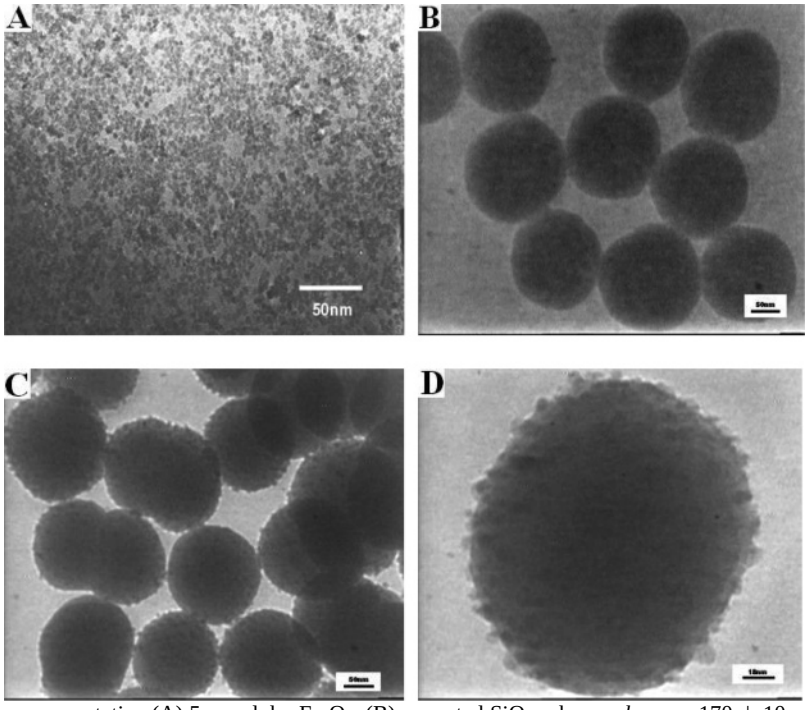

Figure 2. TEM images of the representative (A) 5 nm alpha-Fe_2O_3; (B) uncoated SiO_2 spheres, $d_{sphere} = 170 \pm 10$ nm; (C) Alpha-Fe_2O_3 adsorbed on the surface of SiO_2 spheres taken at a low magnification; (D) Alpha-Fe_2O_3 adsorbed on the surface of SiO_2 spheres taken at a high magnification.

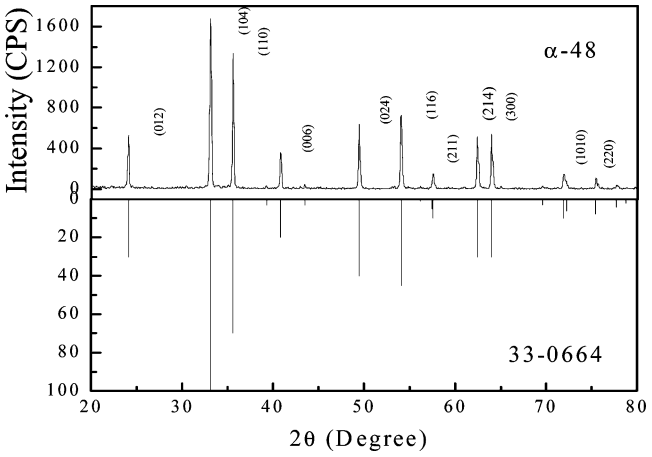

Figure 3. X-ray diffraction patterns of the 48 nm α-Fe_2O_3 nanoparticles.

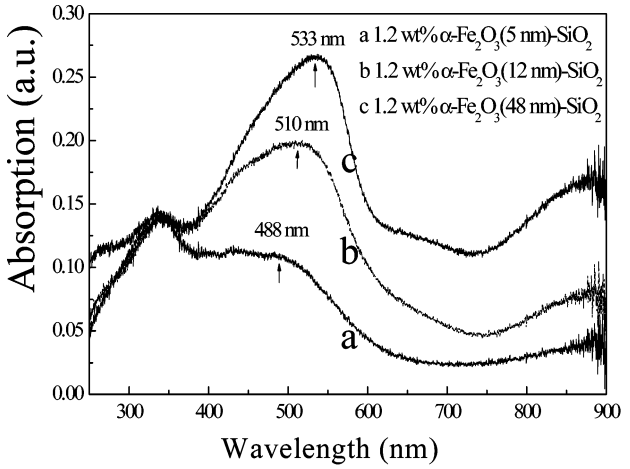

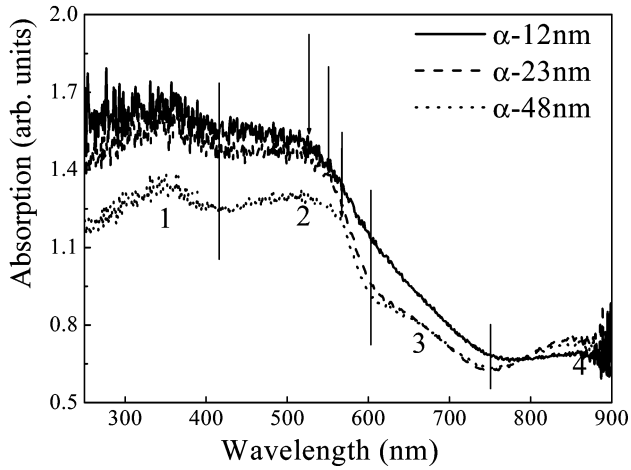

Figure 4. (a) Absorption spectra of the α-Fe_2O_3 nanoparticles of different sizes coated on SiO_2 spheres with 1.2 wt %. (b) Absorption spectra of the α-Fe_2O_3 nanoparticles of different sizes.

wavelength for larger particles. However, we find the reflectivity produces reverse behavior in the Fe_2O_3/SiO_2 composites; the reflectivity of larger particles becomes smaller. This indicates that the absorption intensity of the composite in the 400−600 nm region is much larger than that in the 250−400 nm region, especially for those large-sized nanocrystals (in Figure 4a). Hence the absorption enhancement in the longer wavelength region for 48 nm nanocrystals reflects a photonic crystal effect because the intrinsically enhanced scattering for large particles was overcome by the photon localization.[30−32]

For the nanocrystal sol, the absorption intensity increases with decreasing wavelength. The absorption coefficients of Fe_2O_3 nanocrystals in the range of 600−900 nm are minor for real nanosytems.[33] For nanocrystal aggregates, the weak absorption band in that region was shown in Figure 4b due to the d−d transition. Equally importantly, the transition of 400−600 nm changes much due to the combination of Fe_2O_3 nanocrystals and SiO_2 microspheres. Comparing Figure 4a and Figure 4b, one can find that a nontrivial enhancement of absorption intensities in longer wavelength regions between 400 nm and 600 nm occurred with particle size increase. In addition to those intensity changes, the size-related absorption band edge shifts

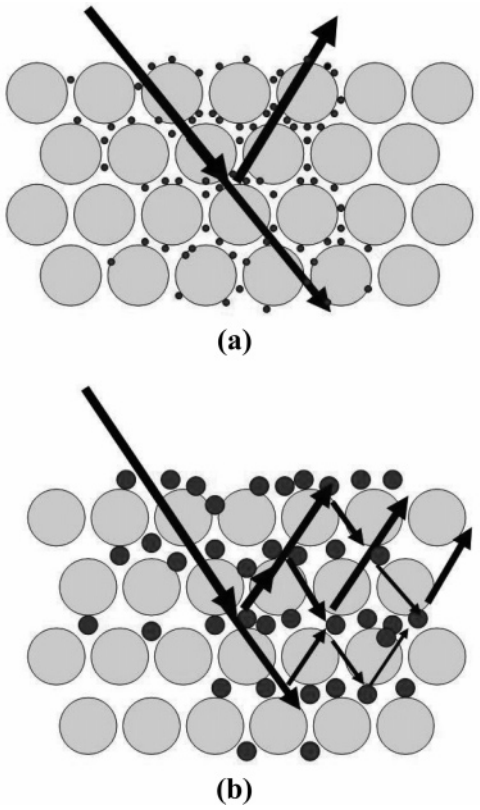

Figure 5. (a, b) Photon movement path in SiO_2 microsphere array with varied sized Fe_2O_3 nanocrystals.

can be clearly observed to move from 533 to 488 nm with the particle size decreased from 48 to 5 nm. This quantum size effect could account for this shift for a delocalized band, which is crucial for the photovoltaic effect of such a quantum-confined semiconductor. This result indicates that the electronic states in this energy range are not completely localized, i..e., cannot be accounted for by local transitions. The increasing magnetic tilt coupling in large alpha-Fe_2O_3 leads to the pair excitons, and the pair exciton looks to be a combination of local d−d transition and charge-transfer band tails. The latter is exactly what is need for the delocalized state to produce photovoltaic responses. In the fs pump−probe technique, we clearly observed the positive absorption of narrow local transition to transform to a broad pair exciton band with time progression, which indicates the natural difference of these transitions. The pair exciton covers the superexchange between neighboring Fe(III) ions, so the charge transfer takes part in the pair exciton formation.[33] We can also see that the relative intensity between 600 and 900 nm changes with varying particle sizes, which is related to the magnetic local correlation between the transition metal ions, i.e, a finite size effect,[33] but this transition gives no photovoltaic response.

The abnormal enhancement of the 400−600 nm band clearly occurred due to the SiO_2 microsphere array, which may introduce a multiscattering process in the light absorption such as an imperfect photonic crystal,[32] as shown in Figure 5a and 5b. For our SiO_2 sphere film, sometimes we can find an asymmetrical transition band in the range of 370−400 nm after long-time, careful drying of the sol on quartz and using thin light spot to detect the transmission spectra (see Supporting Information), which is similar to the transmittance and reflectance spectra of SiO_2 spheres reported by ref 34. This band does not agree exactly with the Bragg diffraction predictions, but the result reflects a photonic crystal effect. So we can consider

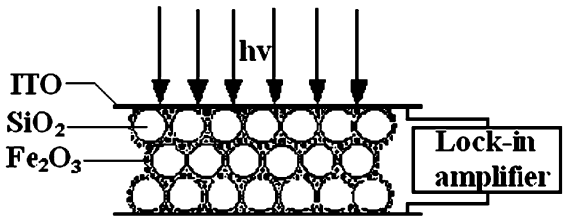

Figure 6. Schematic representations of solid-junction photovoltaic cell indium tin oxide(ITO)/sample/ITO sandwich structure.

that this effect can extend to the Fe_2O_3/SiO_2 composite, though the composite cannot be studied with the transmittance measurement for low transmittance. At first, the excitation light can penetrate the surface-adsorbed Fe_2O_3 nanocrystals to a definite depth and go into the SiO_2 microsphere arrays, where the light could undergo multiple penetration, scattering, and reflectance steps in sphere arrays, which would enhance the absorbance of Fe_2O_3 nanocrystals on the surface of microspheres during each penetration and reflectance many times along the long optical path;[35] hence, this long optical path leads to large absorption coefficients. This process should work with suitably large sized particles of several tens (generally over 20 nm) of nanometers or larger because the larger particles reflect and scatter light more effectively than the very small particles. We can consider the composite in one layer coating of Fe_2O_3 nanocrystals on SiO_2 sphere by electrostatic attraction, so more layers are prohibited by the coulomb repulsion. For 5 nm, the aggregate of two particles gives 10 nm size, so the scattering effect shows a minor effect on the absorption spectra of Fe_2O_3. For 12 nm particles, the scattering taking place for the size of two neighboring particles is over 20 nm, so the absorption enhancement can be observed. For 48 nm, the scattering becomes more important than previous two composites, and its absorption spectra get even more enhanced. Moreover, the enhanced bands show red shift, which is because the photonic band gap moves to long wavelength if the sphere size becomes large,[34] and the size of composite is determined not only by the SiO_2 sphere itself but also by the size of the two particles that have to be taken into consideration. So as the whole composite particle goes larger, the enhanced band moves to longer wavelength as in Figure 4a. This phenomenon cannot be accounted for by the Rayleigh scattering because the short wavelength light should be scattered more intensely in this case. Therefore it is possible to design more powerful microstructures for increasing light absorption efficiency in special applications such as solar cells.

C. Surface Photovoltage Specroscopy (SPS) Measurements. Surface photovoltage spectroscopy (SPS) measurements were carried out with a solid-junction photovoltaic cell indium tin oxide(ITO)/sample/ITO sandwich structure as shown in Figure 6. It is ensured that the light penetrating depth is much less than the thickness of the sample. A lock-in amplifier synchronized with a light chopper was employed to amplify the photovoltage signals. The principle of this SPS measurement had been used successfully to study nanosystems and semiconductors in refs 36−37. SPS of sample A (5 nm), B (12 nm), and C (48 nm) are shown in Figure 7. There are clear SPV response band edges at 400, 500, and 550 nm, respectively, for the 5, 12, and 48 nm Fe_2O_3 nanocrystals. This is an obvious quantum size effect. However, a question remains for the differences of Figure 4 and Figure 7; i.e., why do their SPV spectra and absorption spectra show different quantum size effects?

We can use the electronic structure diagram in Figure 8 to analyze the difference between Figure 4 and Figure 7. For

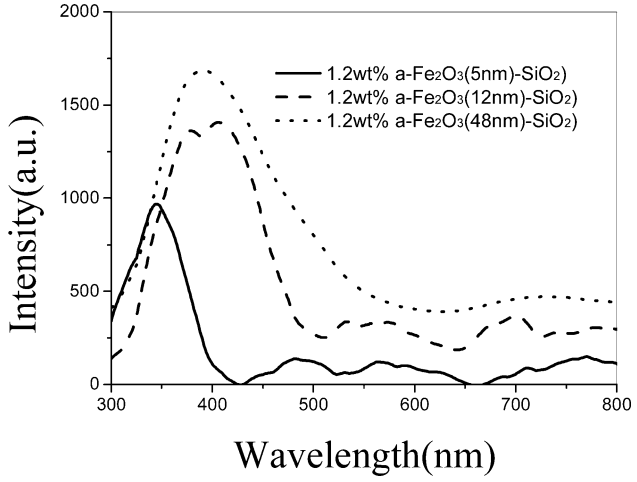

Figure 7. Surface photovoltage spectra of the α-Fe_2O_3 nanoparticles of different sizes coated on SiO_2 spheres with 1.2 wt %.

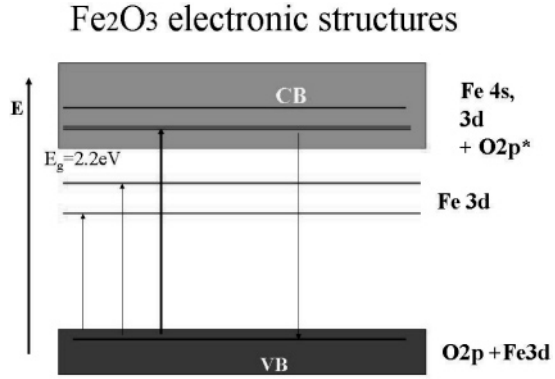

Figure 8. Electronic structure of Fe_2O_3.

absorption spectra, all types of transitions contributed to the absorption coefficients (optical density), the local and delocalized (continuum) transitions all could show up in Figure 4. For SPV spectra, the situations are a little complicated, but only the continuous band and electronic transport contributes to the SPV responses. In principle, one nanocrystal cannot produce a steady photovoltaic response because there is no band-bending on the surface of nanocrystals due to limited space and the change of electronic distribution under light illumination, and because the photoinduced electron−hole cannot separate within a small distance for enough time to be detected by electrodes far away. So the SPV responses in Figure 7 should be understood in a new consideration. In the Fe_2O_3−SiO_2 composite structures shown in Figure 6, we can deduce that the SPV responses should be produced by the following process: Fe_2O_3 nanocrystals absorb light to produce electrons and holes with local and delocalized transitions; for the latter transition the separated electrons or holes could move over some other nanocrystals via delocalized bands in different way, which causes the charge separation of electron and hole. So there occurs an electron (or charge) density difference between the illuminated zone and un-illuminated zones. This carrier density difference would produce SPV responses. From Figure 8 and Figure 4, we can see that the local transitions contribute significantly to the optical absorption processes; however, our SPV spectra proved that the charge-transfer band (CT) is the dominant contribution of photovoltaic responses for 5 nm particles, which is in agreement with the results in ref 6. For 12 nm and 48 nm, we can see the red shift with rising size contributed by the pair exciton due to the d−d transition enhancement. As indicated by the fs spectra,[33] the pair exciton cannot avoid the CT band tail and magnetic coupling. Hence the clear size effect of SPV responses in Figure 7 represents a shift of charge-transfer band and band tail extension with the particle size, while the intrinsic d−d transition did not produce itinerant carriers (610−900 nm) for the SPV signal. The pair excitons as well as the CT band tail in 400−600 nm can produce some itinerant carriers for SPV signals, whose shift with size clearly proved that the quantum confinement occurred on the delocalized band in Fe_2O_3 nanocrystals. Finally, the optical absorption and SPV spectra become unity for large nanocrystal composites.

Conclusion

By comparing the optical absorption and SPV spectra, we can observe a clear quantum size effect of alph-Fe_2O_3 nanocrystals dispersed on the surface of silica colloidal spherical particles. The absorption and SPV of alpha-Fe_2O_3 nanocrystals are quite different for small sizes but are similar for large nanocrystals. The SPV response of alpha-Fe_2O_3 can be accounted for by the electron transition from O_{2p} (valence band) to conduction band (hybridized band) and band tail accompanied by the pair excitons, in contrast to the miscellaneous transitions in optical absorption. It is interesting to indicate that the visible optical transition coefficients can be enhanced by introducing SiO_2 microsphere photonic crystals as the skeleton for nanostructure architecture. This technique may be useful for future solar cell design.

Acknowledgment. The authors would like to thank the nanofund of Hunan University, the National Natural Science Foundation of China under Grant (No. 20173073, No. 90306010 and 20371015), 973 project (2002CB713802), and Program for New Century Excellent Talents in University of China.

Supporting Information Available: Transmittance spectrum of SiO_2 thin film by 170 nm microsphere. This material is available free of charge via the Internet at http://pubs.acs.org.

References and Notes

(1) Alivisatos, A. P. *Science* **1996**, *271*, 933.
(2) Brus, L. E. *J. Chem. Phys.* **1984**, *80*, 4403.
(3) Klimov, V. I.; Mikhailovsky, A. A.; Xu, S.; Malko, A. *Science* **2000**, *290*, 314.
(4) Baetzold, R. C.; Yang, H. *J. Phys. Chem. B* **2003**, *107*, 14357.
(5) Pileni, M. P. *J. Phys. Chem.* **2001**, *105*, 3358.
(6) Du, H.; Cao, Y.; Bai, Y. B.; Zhang, P.; Qian, X. M.; Wang, D. J.; Li, T. J.; Tang, X. Y. *J. Phys. Chem. B* **1998**, *102*, 2329.
(7) Cherepy, N. J.; Liston, D. B.; Lovejoy, J. A. *J. Phys. Chem. B* **1998**, *102*, 770.
(8) Ziolo, R. F.; Giannelis, E. P.; Weinstein, B. A. *Science* **1992**, *257*, 219.
(9) Chien, C. L. *J. Appl. Phys*. **1991**, *69*, 5267.
(10) Ennas, G.; Musinu, A.; Piccaluga, G.; Zedda, D. *Chem. Mater*. **1998**, *10*, 495.
(11) Tartaj, P.; Gonzalez-Carreno, T.; Serna, C. J. *J. Phys. Chem. B* **2003**, *107*, 20.
(12) Kronik, L.; Shapira, Y. *Surf. Sci. Rep.* **1999**, *37*, 1−206.
(13) Tengfeng, X.; Dejun, W.; Lianjie, Z.; Ce, W. *J. Phys. Chem. B* **2000**, *104*, 8177.
(14) Leibovitch, M.; Kronik, L.; Fefer, E.; Shapira, Y. *Phys. Rev. B* **1994**, *50*, 1739.
(15) Yanhong, L.; Dejun, W.; Qidong, Z.; Min, Y. *J. Phys. Chem. B* **2004**, *108*, 3202.
(16) Lenzmann, F.; Krueger, J.; Brooks, S. *J. Phys. Chem. B* **2001**, *105*, 6347.
(17) Xie, T. F.; Wang, D. J.; Zhu, L. J.; Li, T. J. *J. Mater. Chem. Phys.* **2001**, *70*, 103.
(18) El-Sayed, M. A. *Acc. Chem. Res.* **2004**, *37*, 326−333.
(19) Mittleman, D. M.; Schoenlein, R. W.; Shiang, J. J.; Colvin, V. L.; Alivisatos, A. P.; Shank, C. V. *Phys. Rev. B* **1994**, *49*, 14435−14447.

(20) Burda, C.; Link, S.; Mohamed, M.; El-Sayed, M. A. *J. Phys. Chem. B* **2001**, *105*, 12286.
(21) Kan, S. H.; Yu, S.; Peng, X. G.; Zhang, X. T.; Li, T. J. *J. Colloid Interface Sci*. **1996**, *178*, 673.
(22) Saric, A.; Music, S.; Nomura, K. *Mater. Sci. Eng. B* **1998**, *56*, 43.
(23) Sapieszko, R. S.; Matijevic, E. *J. Colloid Interface Sci*. **1980**, *74*, 405.
(24) Stöber, W.; Fink, A.; Bohn, E. *J. Colloid Interface Sci*. **1968**, *26*, 629.
(25) Kosmulski, M.; Matijevic, E. *Langmuir* **1991**, *7*, 2066.
(26) Ohmori, M.; Matijevic, E. *J. Colloid Interface Sci*. **1992**, *150*, 594.
(27) Sherman, D. M.; Waite, T. D. *Am. Mineral*. **1985**, *70*, 1262.
(28) Hashimoto, T.; Yamada, T.; Yoko, T. *J. Appl. Phys*. **1996**, *80*, 3184.
(29) Burda, C.; Chen, X. B.; Narayanan, R.; El-Sayed, M. A. *Chem. Rev*. **2005**, *105*, 1025−1102.
(30) Reichelt, M.; Pasenow, B.; Meier, T.; Stroucken, T.; Koch, S. W. *Phys. Rev. B* **2005**, *71*, 035346.
(31) Lin, S. Y.; Fleming, J. G.; Li, Z. Y.; El-Kady, I.; Biswas, R.; Ho, K. M. *J. Opt. Soc. Am*. **2003**, *20*, 1538.
(32) Bakueva, L.; Musikhin, S.; Sargent, E. H.; Ruda, H. E.; Shik, A. *Handbook of Organic−Inorganic Hybrid Materials and Nanocomposites*; Nalwa, H. S., Ed.; American Scientific Publishers: Stevenson Ranch, CA, 2003; Vol. 2, chapter 5, pp 181.
(33) He, Y. P.; Miao, Y. M.; Li, C. R.; Wang, S. Q.; Cao, L.; Xie, S. S.; Yang, G. Z.; Zou, B. S.; Burda, C. *Phys. Rev. B* **2005**, *71*, 125411.
(34) Shin, D. C.; Kim, M. S.; Y. T. O, Hong, S. J.; Lee, B. G. *Proc. SPIE*, 5733, 4502005.
(35) Lin, Y.; Zhang, J.; Sargent, E. H.; Kumacheva, E. *Appl. Phys. Lett*. **2002**, *81*, 3134.
(36) Wang, D. J.; Zhang, J.; Shi, T. S.; Wang, B. H.; Cao, X. Zh.; Li, T. J. *J. Photochem. Photobiol. A: Chem.* **1996**, *93*, 21.
(37) Lin, Y. H.; Wang, D. J.; Zhao, Q. D.; Yang, M.; Zhang, Q. L. *J. Phys. Chem. B* **2004**, *108*, 3202.